ARTICLE IN PRESS

Tetrahedron xxx (xxxx) xxx

Contents lists available at ScienceDirect

Tetrahedron

journal homepage: www.elsevier.com/locate/tet

AIE activity, mechanochromic property and solvent inclusion of two β-diketones with tetraphenylethylene unit

Jianfeng Jiang [a], Yongtao Wang [a, *], Lei Ma [b], Xueming Li [a, **], Xiaojuan Wang [a, ***], Yanjun Guo [a]

[a] Guangxi Key Laboratory of Electrochemical and Magneto-chemical Function Materia, College of Chemistry and Bioengineering, Guilin University of Technology, Guilin, 541004, PR China

[b] Tianjin International Center for Nanoparticles and Nanosystem, Tianjin University, Tianjin, 300072, PR China

ARTICLE INFO

Article history:
Received 12 October 2022
Received in revised form
1 March 2023
Accepted 3 March 2023
Available online xxx

Keywords:
Mechanochromism
AIE
β-diketone
Solvatochromism
Internal mechanism

ABSTRACT

Highly twisted molecular conformation easily leads to the loose molecular packing and big voids, which are desirable for mechanochromism and solvent inclusion. Here, **TPE-BF** and **TPE-BT** with highly twisted molecular conformation were designed and synthesized by α-substitution of two β-diketonates. **TPE-BF** and **TPE-BT** show similar aggregation-induced emission activity, but different mechanochromism. Subsequently, the corresponding internal mechanism are analyzed and discussed in-depth by XRD, DSC, fluorescence lifetime, crystal analysis and theoretical calculation. Compared with crystal **TPE-BF**, crystal **TPE-BT** exhibits more obvious mechanochromism (red shift of 12 nm) before/after grinding, which is attributed to EtOAc inclusion and different intermolecular interactions and stacking. Furthermore, wavelength shifts of **TPE-BF** and **TPE-BT** do not exceed 35 nm after phase transition from crystalline state to amorphous state. Obviously, highly twisted molecular conformations fail to bring about high-contrast mechanochromism (wavelength shift above 100 nm), whose reason should be the suppressed intermolecular π-π interactions and overlap before/after grinding. Combined with previous research results of our laboratory, the luminogens forming solvent inclusion generally have twisted molecular conformation, and similar structural fragment with solvent molecule, which will provide a potential design strategy for selective solvent inclusion.

1. Introduction

By filling channels/voids of crystal lattice, as well forming intermolecular interactions with crystal lattice, solvent molecules are included in the crystal lattice known as solvent inclusion, leading to various properties such as mechanics, solubility, stability, bioavailability [1]. Thereby, solvent inclusion provides a possibility to tune product properties without changing chemical structure of molecules, meanwhile, it can be used as purification and separation of pharmaceuticals, chemical sensing, and capture of volatile harmful solvents [2]. Now, over the last few decades, some scientists have tried to tune photoluminescence of chromophores by solvent inclusion and release in crystalline lattice, but the research on this aspect is still rare [3].

Mechanochromic fluorescence (MCF) materials as research hotspots have been widely reported, which is of great importance for fundamental research and potential application in the fields of stress sensor, damage detection and anti-counterfeiting [4]. MCF materials can change their own spatial conformation, intermolecular arrangement and stacking, as well intermolecular hydrogen bonds and weak interactions under external mechanical forces, generating variant fluorescence signals such as wavelength, intensity, and lifetime [5]. Currently, AIE luminogens have become an important source of MCF materials. The AIE luminogens usually have twisted spatial conformation leading to the loose molecular stacking, which is easy to be destroyed under mechanical force such as grinding, scraping, and compressing [6]. Furthermore, the loose molecular stacking contributes to provide channels or voids for solvent molecules, thereby designing aggregation-induced

* Corresponding author.
** Corresponding author.
*** Corresponding author.
E-mail addresses: wyt_shzu@163.com (Y. Wang), lei.ma@tju.edu.cn (L. Ma), lixueming@glut.edu.cn (X. Li), wangxiaojuan0117@163.com (X. Wang), guoyanjun2516@glut.edu.cn (Y. Guo).

https://doi.org/10.1016/j.tet.2023.133355
0040-4020/

Please cite this article as: J. Jiang, Y. Wang, L. Ma *et al.*, AIE activity, mechanochromic property and solvent inclusion of two β-diketones with tetraphenylethylene unit, Tetrahedron, https://doi.org/10.1016/j.tet.2023.133355

emission (AIE) luminogens with highly twisted molecular conformation will be conducive to explore inclusion of solvent molecules and the resulting mechanochromism [7].

Recently, some difluoroboron β-diketonate complexes (BF_2bdks) and β-diketonates ligands (bdks) had been designed and synthesized by furnishing propeller-like tetraphenylethylene (TPE), furan, thiophene and pyrrole units with isomerism effects [8]. However, crystal analyses reveal these BF_2bdks and bdks generally maintain planar configuration between dioxaborine ring and 1, 3-disubstituted aromatic rings. By Br, CH_3 or methoxyphenyl substitution on α position of dioxaborine ring, the planar configuration between dioxaborine ring and 1, 3-disubstituted aromatic rings become distorted [9]. To yield more distorted molecular conformations, here, two bdks were designed and synthesized by assembling propeller-like TPE unit and benzyl substituent, named as **TPE-BF** and **TPE-BT** respectively (Scheme 1). As expect, **TPE-BF** and **TPE-BT** show remarked AIE activity and highly twisted molecular conformation, but which do not bring about high-contrast mechanochromism before/after grinding, heating, fuming, and curing. Generally, highly twisted molecular conformation easily produces a loose molecular stacking, which is conductive to molecular embedding, recognition, and the resulting isolation and purification. The crystal analysis results indicate ethyl acetate (EtOAc) is selectively embedded in the lattice of crystal **TPE-BT** rather than crystal **TPE-BF**, although they have similar molecular structure. Based on ^{1}H NMR, ^{13}C NMR, UV–vis absorption and emission spectra, XRD, DSC, fluorescence lifetime, single crystal analysis and theoretical calculation, similar AIE activity, and different mechanochromism and solvent inclusion between **TPE-BF** and **TPE-BT** are analyzed and discussed in depth.

2. Results and discussion

The UV–vis spectra of **TPE-BF** and **TPE-BT** mainly contain two absorption bands, whose strong absorption band at 200–320 nm should be ascribed to benzyl, acetyl-furan and acetyl-thiophene moieties, while weak absorption band comes from acetyl-TPE moiety. The absorption maxima show small red shift with the increase of solvent polarity, hinting small dipole moment change in ground state (Fig. 1A–B) [10]. Under the excitation of 338 nm, **TPE-BF** show weak fluorescence emission, accompanied by continuous vibration of emission spectra (Fig. 1C). By contrast, significantly enhanced fluorescence emission can be observed for **TPE-BF** and **TPE-BT** under 250 nm excitation (Table S1). Furthermore, the signal for the C=C–OH residual proton exceeding 10.0 ppm cannot be found in ^{1}H NMR spectra (Figs. S8 and S10), and there are four carbonyl carbons at 194.52, 194.29, 184.16 and 188.01 ppm in ^{13}C NMR spectra (Figs. S8 and S10), which inferred that **TPE-BF** and **TPE-BT** adopt ketone form rather than enol form in $CDCl_3$. Compared with **TPED2F** and **TPED2T** [10], absorption and emission maxima of **TPE-BF** and **TPE-BT** show hypsochromic-shift ascribed to α-substitutions effects, which leads to more twisted molecular configurations and enol-ketone tautomerism inhibition. Thereby, benzyl group destroys the conjugation between TPE and furan/thiophene unit, which is not conducive to the electronic delocalization, leading to weak fluorescence emission, while fluorescence at 250 nm excitation should come from local emission of **TPE-BF** and **TPE-BT**.

Generally, the twisted molecular configuration can enhance the solid-state fluorescence emission performance by reducing the intermolecular π-π stacking and non-radiation energy loss. Presently, increasing non-planarity of molecular configuration has become a highly efficient way to get AIE and mechanochromic luminogens by assembling planar perylene bisimide, boron-dipyrromethenes and BF_2bdks with propeller-like TPE [11]. Even so, the twisted molecular configuration is not a necessary and sufficient condition for AIE activity and mechanochromism. Fortunately, the remarkable AIE characteristics are presented for two luminogens (Fig. 2). Compared with weak fluorescence emission in pure THF, fluorescence intensity started to enhance

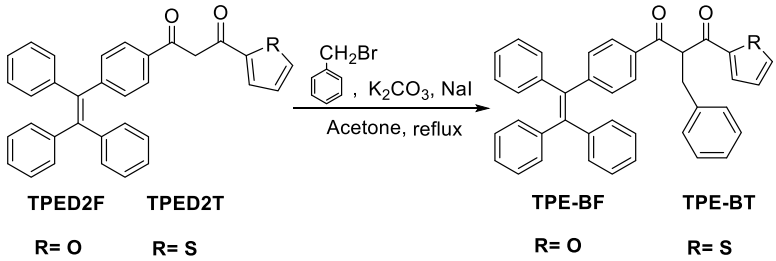

Scheme 1. Synthetic routes of **TPE-BF** and **TPE-BT**.

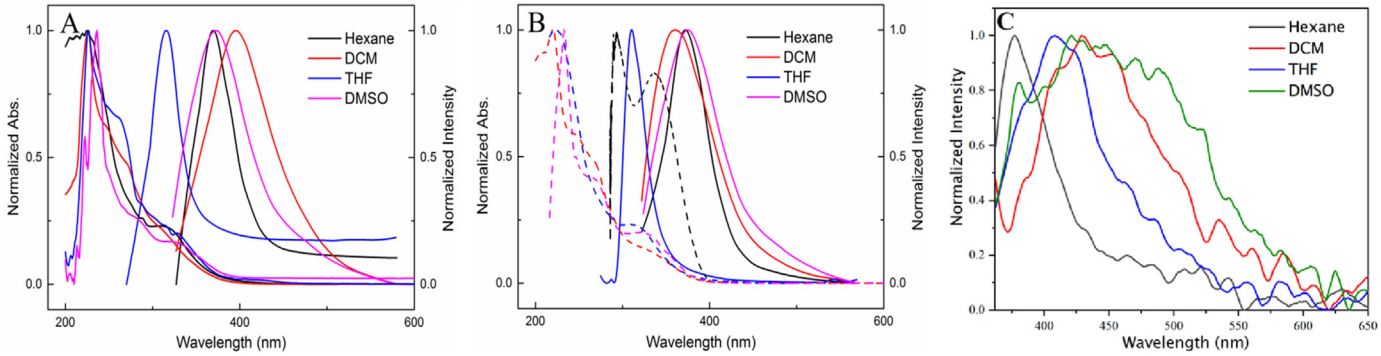

Fig. 1. Normalized UV–vis and fluorescence spectra of (A) **TPE-BF**, (B) **TPE-BT** in various solvents (Solution concentration: 10 μM, Excitation wavelength: 250 nm) (C) Fluorescence spectra of **TPE-BF** in various solvents, Excitation wavelength: 338 nm.

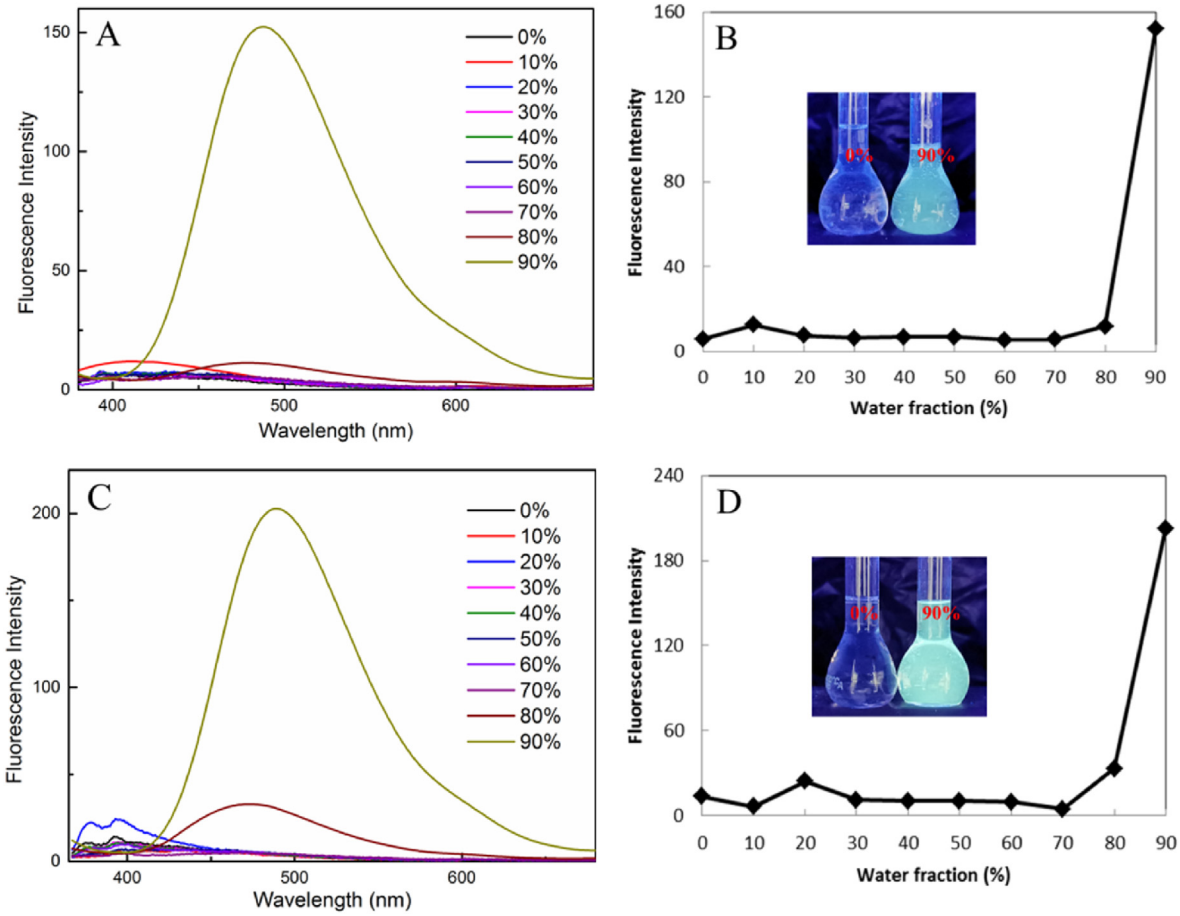

Fig. 2. Fluorescence emission spectra of (A) **TPE-BF**, (C) **TPE-BT** in the THF/water mixtures with different fractions of water. Solution concentration: 10 μM. Chart of relationship between FL peak intensity and water fraction for (B) **TPE-BF**, (D) **TPE-BT**. Solution concentration: 10 μM. (Inset: Photographs in THF/water mixtures with different fractions of water under 365 nm UV illumination). Normalized UV–vis absorption spectra (E) and fluorescence spectra of **TPE-BF** (F) in various solvents. Solution concentration: 10 μM.

accompanied by an obvious redshift of emission wavelength when water fraction (f_w) is up to 80% in mixed solution of THF/H_2O, when f_w reaches 90%, the two dyes exhibited extreme emission enhancement, which depends on the J-type molecular stacking suppressing the non-radiative energy loss of C–C bond rotation and promoting red-shift of wavelength. The similar AIE characteristic has been clarified by adjusting the viscosity of solvents, and nanoparticles of aggregation state are investigated by dynamic light scattering and transmission-electron-microscopy. By using quinine sulfate as the reference [12], the relative fluorescence quantum yields (PLQYs) of **TPE-BF** (0.14) and **TPE-BT** (0.07) were determined at f_w = 90% (S14). Obviously, the PLQYs of the two luminogens are still very low even in the aggregated state, which should be attributed to their highly twisted molecular conformation. Besides, emission maxima of **TPE-BT** have a bathochromic shift compared with that of **TPE-BF** due to isomerism effects of furan and thiophene units.

Furthermore, it's worth looking forward to whether the highly twisted configuration can produce mechanochromism. Crystal **TPE-BF** and **TPE-BT** are obtained by slowly volatilizing the mixed solution of n-hexane and CH_2Cl_2, depressively, **TPE-BF** does not exhibit mechanochromic performance at all based on the contrast of the fluorescence emission maxima before/after grinding (Figs. 3 and 4). Different from **TPE-BF**, **TPE-BT** show 12 nm bathochromic-shift before/after grinding, even if the mechanochromic property is not ideal, it is still fascinating that two similar molecular structures show different mechanochromism. Next, mechanochromic

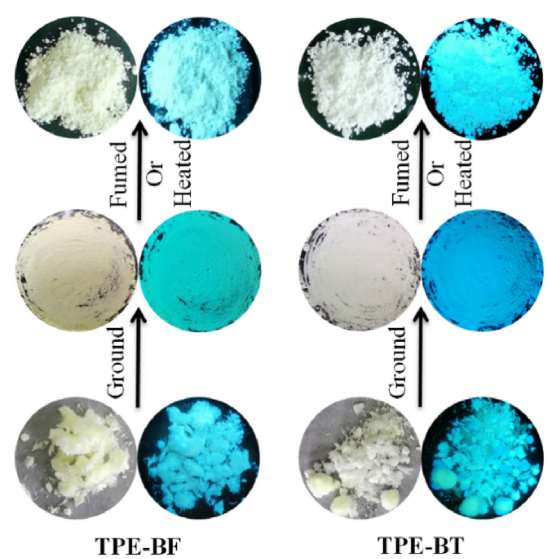

Fig. 3. Photographic images of TPE-BF, TPE-BT in different solid states under natural light and UV light (365 nm).

reversibility of **TPE-BT** is examined by annealing (110 °C) and solvent fuming. The results indicate that emission maxima of ground **TPE-BT** gives the same blue shift by heating and CH_2Cl_2 fuming,

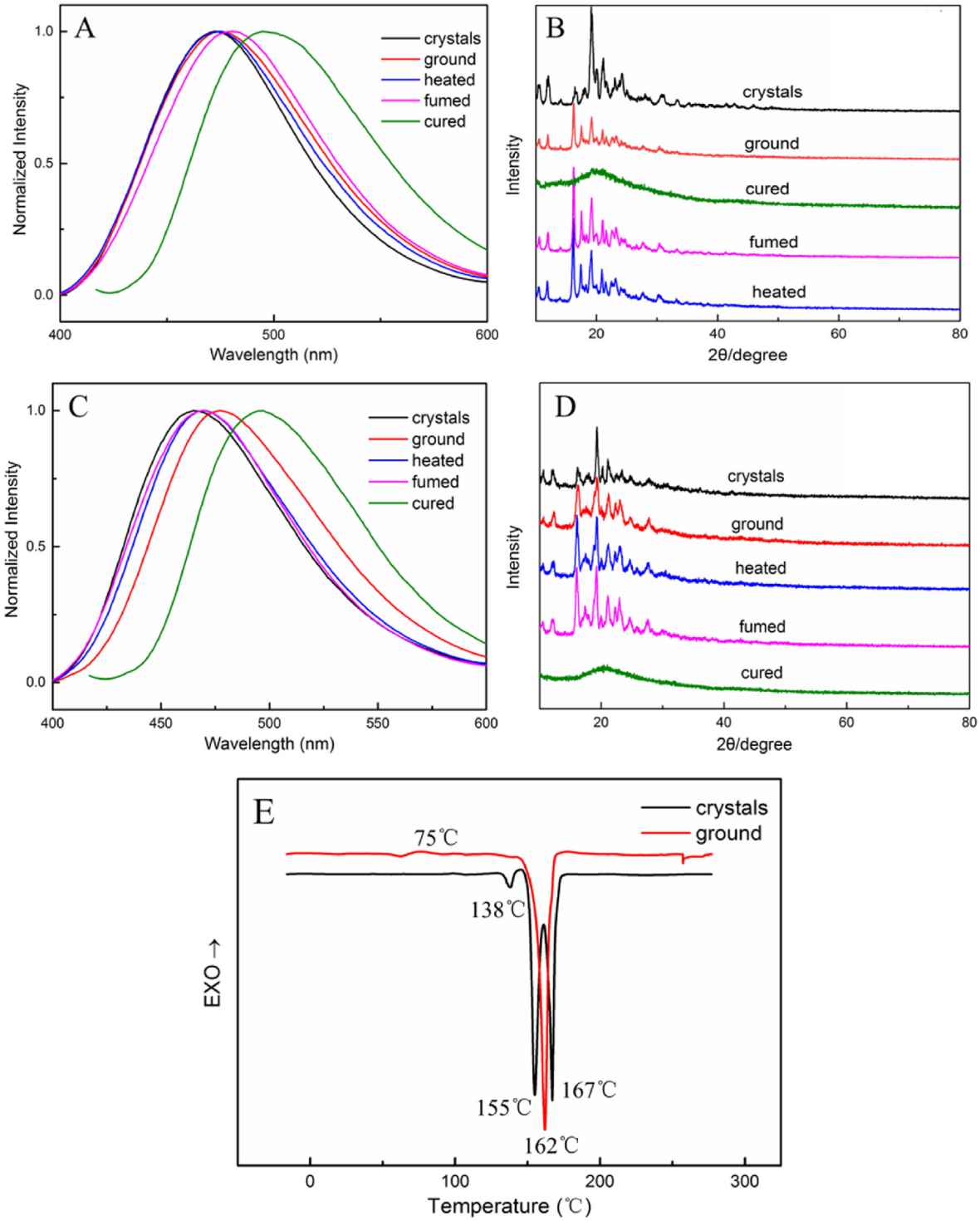

Fig. 4. Fluorescence spectra of complex of (A) **TPE-BF**, (C) **TPE-BT** in different solid states (cured: after the crystal is melted, it is placed in liquid nitrogen for quenching), and XRD patterns of (B) **TPE-BF**, (D) **TPE-BT** in various solid states. DSC thermograms of (E) **TPE-BT** crystals in different state.

while ground **TPE-BF** can response to solvent fuming but not to heating, however, these wavelength shifts do not exceed 10 nm. To further explore the intrinsic mechanism of the above discrepancy, we firstly carried out X-ray diffraction (XRD) analysis. XRD spectra confirm that both **TPE-BF** and **TPE-BT** maintain crystalline state before/after grinding, heating and solvent fumigation (Fig. 4B and D). Furthermore, **TPE-BF** and **TPE-BT** show different XRD spectra before/after grinding. For the former, the diffraction peaks near 20° present a clear blue shift from crystal to ground sample. Yet the latter grinding alters the relative intensity of diffraction peaks at 15° and 19°. In differential scanning calorimetry (DSC) curve of ground **TPE-BT,** the exothermic peak belonging to cold-crystallization transition is not detected, which mean that grinding does not produce the meta-stable state (Fig. 4). Crystal **TPE-BT** has two melting points at 155 °C and 167 °C, but only one melting point at 162 °C in ground **TPE-BT** sample, which should be

attributed to homogenization of crystal particles after grinding. In addition, there are two endothermic peaks at 138 °C and 75 °C in crystal and ground **TPE-BT** samples respectively because of the escape of ethyl acetate (EtOAc). The escape temperature is higher than the boiling point of EtOAc due to long diffusion distance and the intermolecular interactions between the crystal and EtOAc (Fig. S7), while grinding reduces crystal size and exposes part of EtOAc to the outside, leading to the escape temperature is close to the boiling point of EtOAc. Thereby, the inferior mechanochromic properties of **TPE-BF** should be attributed to crystalline-to-crystalline phase transition changing the local molecular layer spacing, but effect of the phase transition on molecular conjugation is inconspicuous. Compared with **TPE-BF**, the more obvious mechanochromism lies in the formation of EtOAc inclusion. Similarly, tiny fluorescence emission wavelength shift induced by heating and fuming is also attributed to similar intermolecular arrangement and stacking, which can be judged from identical XRD spectra. The fluorescence lifetime decay curve of crystal **TPE-BF** and **TPE-BT** contain two exponential components with average fluorescence lifetime of 4.59 ns and 4.87 ns in turn, which is consistent with their crystal density (Figs. S1–3). Compared with **TPE-BF** (1.248 g cm^{-3}), higher crystal density for **TPE-BT** (1.257 g cm^{-3}) can prolong fluorescence life by inhibiting rotation and vibration of C—C bonds. After grinding, the short lifetime and the long lifetime of **TPE-BT** show slight variations, but average fluorescence lifetime keep constant (Figs. S1–4), which is in accord with identical XRD spectra before/after grinding. Based on theoretical calculation by extracting molecule from single crystal, as shown in Fig. 5, the electron density distribution of the highest occupied molecular orbital (HOMO) mainly located at TPE unit, while the electron density distribution of lowest unoccupied molecular orbital (LUMO) mainly located at furan, thiophene and β-diketone units, indicating obviously ICT effect.

Single crystal X-ray analysis confirmed that **TPE-BF** (CCDC 1994664) **and TPE-BT** (CCDC 1994673) possess highly distorted molecular configurations and varied weak intermolecular interactions (Fig. 6, Figs. S5 and S6). Crystal **TPE-BF** is a triclinic system with the space group P1 [a = 5.4828(6) Å, b = 9.4168(12) Å, and c = 29.638(4) Å; α = 987.527(5)°, β = 91.125(4)°, and γ = 100.343(3)°]. Crystal **TPE-BT** is a monoclinic system with the space group 21/*c* [a = 10.1555(9) Å, b = 10.2361(8) Å, and c = 16.8532(15) Å; α = 90°, β = 90.154(3) °, and γ = 90°]. Especially, one benzyl substituent of **TPE-BF** can form 10 intermolecular hydrogen bonds and weak interactions with neighboring molecules, for single **TPE-BF** molecule, the number of intermolecular hydrogen bonds and weak interactions are up to 32. When ground **TPE-BF** is heated, the strong intermolecular interactions is not easy to be destroyed, leading to stable emission maxima before/after heating. Compared with **TPE-BF**, **TPE-BT** contains much less intermolecular hydrogen bonds and weak interactions [13], which facilitate bigger wavelength shift for ground **TPE-BT** than ground **TPE-BF** before/after heating. Forming two planes between two carbonyl groups and their α-carbon are nearly perpendicular, whose dihedral angles are 89.63°, 76.20° and 85.89° for **TPE-BF** and **TPE-BT** respectively. Moreover, the enol form is not found in crystals **TPE-BF** and **TPE-BT**. In other words, benzyl substitution not only destroys the planar structure of β-diketonate, but also inhibits the enol-ketone tautomerism, thereby the whole molecule cannot form effective π-π conjugation, leading to blue shift fluorescence emission. Besides, both **TPE-BF** and **TPE-BT** adopt head-to-head arrangement and side-to-face stacking modes (β-diketone unit is defined as the head), destroying intermolecular electron delocalization. Furthermore, the above factors combined with rigid molecular conformation cause inconspicuous wavelength shift for **TPE-BF** and **TPE-BT** before/after grinding. For comparison, the head-to-head arrangement modes of **TPE-BF** and **TPE-BT** are different**,** as shown in Fig. 6, **TPE-BF** adopts parallel head-to-head stacking, but the head-to-head stacking of **TPE-BT** is zigzag type forming some large voids. The different intermolecular interactions and stacking may be the reason of EtOAc embedded in **TPE-BT**, but not in **TPE-BF** despite they have similar structure and spatial molecular conformation. What's interesting is that EtOAc participates in the ordered arrangement of crystal **TPE-BT**, forming various intermolecular interactions such as C—H···C (2.388 Å and 2.779 Å) and C···C (3.313 Å). EtOAc is in a hydrophobic cavity surrounded by three TPE units and one benzyl group, remaining L-type spatial conformation and the same molar equivalent with **TPE-BT** in crystal (Fig. S13). As speculation, EtOAc embedding should be selective molecular recognition because mixed solvents of two crystals are n-hexane and CH_2Cl_2. Introduction of trace amounts EtOAc should be attributed to purification process of **TPE-BT** by column chromatography (silica gel, 8:1 v/v, petroleum ether/EtOAc). Furthermore, the hydrophobic cavity is formed by intermolecular interactions between EtOAc and two **TPE-BT** molecules, and it is big enough to accommodate n-hexane and CH_2Cl_2, therefore, the selective embedding may be a self-assembling induced by EtOAc. It is worth mentioning that this kind of solvent embedding is not the only one example. In our previous study, methanol (MeOH) and n-hexane were embedded in crystal **TPEDKBF$_2$OMe** and **TPEDKBF$_2$Ono** [14], respectively. More interesting, some rules can be found from these examples. Solvent molecules embedded and side chains of luminogens have similar molecular structures and polarity, for

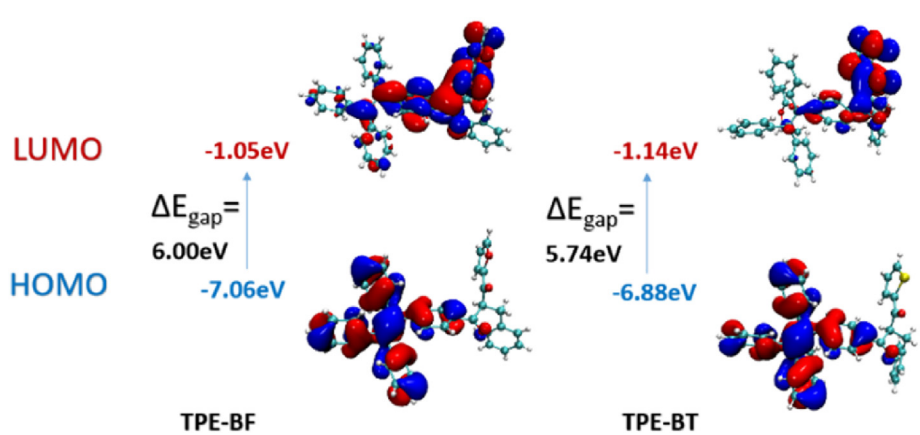

Fig. 5. Molecular orbital amplitude plots of HOMO and LUMO levels for crystal **TPE-BF** and **TPE-BT.**

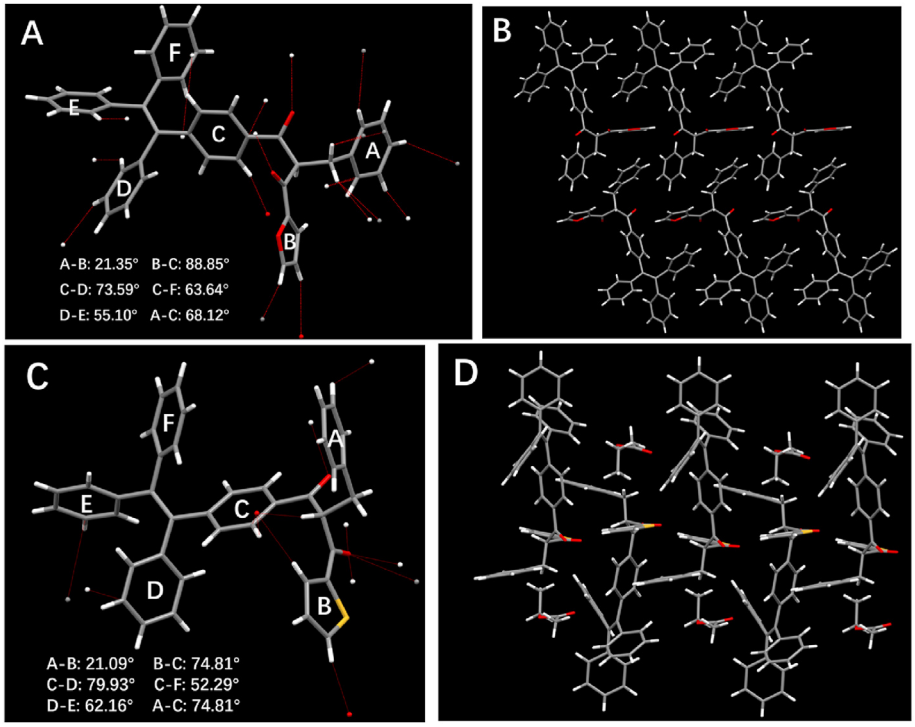

Fig. 6. Single crystal structure of (A) **TPE-BF**, (C) **TPE-BT** and molecular stacking mode of (B) **TPE-BF**, (D) **TPE-BT**.

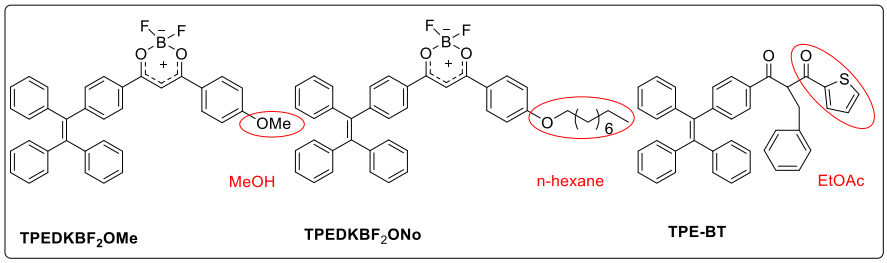

Fig. 7. Similar molecular structures and polarities between solvent molecules embedded and side chains in crystal **TPEDKBF$_2$OMe, TPEDKBF$_2$ONo** and **TPE-BT**.

examples, MeOH and methoxy group of **TPEDKBF$_2$OMe**, n-hexane and nonoxy group of **TPEDKBF$_2$ONo**, and EtOAc and acyl thiophene of **TPE-BT** (Fig. 7). In addition, **TPEDKBF$_2$OMe, TPEDKBF$_2$ONo** and **TPE-BT** occupy twisted molecular configuration and loose molecular stacking. By extracting EtOAc and **TPE-BT** molecules from single crystal, the free energy of solvation between EtOAc and **TPE-BT** is calculated as −0.199 eV, obviously, which is not stable enough for grinding and heating. By contrast, **TPE-BF** without solvent molecules maintains the same fluorescence emission before/after grinding. Thus, mechanochromism of **TPE-BT** is closely related to solvent molecule embedded and relatively weak intermolecular interactions. To further study of mechanochromic properties of the two bdks, amorphous **TPE-BF** and **TPE-BT** are obtained by melting and cooling rapidly with liquid nitrogen, and characterized by XRD spectra, as shown in Fig. 4B and D, two wide diffraction peaks confirm formation of amorphous state. As expected, the two cured samples show more significant redshift compared with the corresponding ground samples. However, the highly twisted spatial conformation and rigid molecular skeleton inhibit intermolecular π-π interactions and head-to-head/tail overlap even in amorphous state, leading to insignificant wavelength shift after grinding.

3. Conclusions

In summary, **TPE-BF** and **TPE-BT** with highly twisted spatial conformation were designed and synthesized. High twisted molecular conformations endow two luminogens with marked aggregation-induced emission enhanced (AIEE) activity by inhibiting intermolecular π-π stacking. The grinding leads to scare crystalline-to-crystalline phase transformation with tiny influence on molecular conjugation, only accompanied by 1 nm and 12 nm wavelength shift for **TPE-BF** and **TPE-BT** respectively. The higher-contrast mechanochromism for **TPE-BT** is attributed to EtOAc embedded. Furthermore, heating and solvent fumigation endow ground **TPE-BT** with the same blue shift for emission wavelength, while ground **TPE-BF** does not response to heating but to solvent fuming ascribed to stronger intermolecular interactions. Compared with the pristine crystals, emission maxima of amorphous **TPE-BF** and **TPE-BT** show bathochromic shifts of 23 nm and 31 nm respectively. Obviously, the highly twisted spatial conformation forbids luminogens to form intermolecular π-π or head-to-head/tail overlap before/after grinding, which is not conducive to enhance the contrast of mechanochromism, however, it is helpful for the formation of loose molecular stacking and voids, generating

solvent embedding. Although **TPE-BF** and **TPE-BT** have similar molecular structure and conformation, **TPE-BT** exhibits different molecular stacking and arrangement, and contains much less intermolecular hydrogen bonds and weak interactions in crystalline state, which may be the reason of EtOAc embedded in **TPE-BT** rather than **TPE-BF**, moreover, the embedding may be a selective molecular recognition, which is related to the structure and polarity of side chain of luminogen.

4. Experimental section

General Considerations: The UV–vis spectra were determined on a Mapada UV-3200pcs spectrophotometer. Fluorescence measurements were taken on Agilent Cary Eclipse fluorescence spectrophotometer. ^{1}H NMR spectra and ^{13}C NMR spectra were obtained with a Varian inova instrument at 400 MHz and 100 MHz using tetramethylsiane (TMS) as the internal standard, and $CDCl_3$ as the solvent in all cases. Glass transition temperature and melting point was measured by carried out DSC measurements using DSC Q2000 (TA, America). MALDI/HRMS were record on an UltrafleXtreme MALDI-TOF/TOF mass spectrometer (Bruker, Germany). Powder XRD measurements were performed on the D8 Advance (Bruker) with Cu Kα radiation in the range of $10^o < 2\theta < 90^o$. Fluorescence lifetimes were measured by using an Edinburgh Instrument FLSP920 fluorescence spectrophotometer, and all the samples were excited at 360 nm. THF, CH_2Cl_2 and acetone were dried according to standardized procedures previously described. All the other chemicals and reagents used in this study were of analytical grade without further purification. In general, all the intermediates and final compounds were purified by column chromatography on silicagel (200–300 mesh), and crystallization from analytical grade solvents. Reactions were monitored by using thin layer chromatography (TLC). According to the reported method, benzophenone was used as a reagent to synthesize TPE; then TPE and acetyl chloride were acylated by Friedel-Crafts to obtain compound TPE-$COCH_3$. Geometries were optimized at the PBE0-D3(BJ) level of theory, including the D3(BJ) correction for intramolecular dispersion. The def2-SVP basis set was employed for all atoms. Frequencies were analytically computed at the same level of theory to confirm whether the structures are minima (no imaginary frequency). Energies were calculated by using the PWPB95-D3 (BJ) method, along with the def2-QZVPP basis sets. The free energy of solvation was calculated at the M052X/6-31G* level of theory. All of the calculations were performed using Gaussian 16 and ORCA 4.2 program package, and the structures and molecule orbitals (MOs) were generated by Multiwfn and VMD.

4.1. 2-Benzyl-1-(furan-2-yl)-3-(4-(1,2,2-triphenylvinyl)phenyl) propane-1,3-dione (TPE-BF)

Adding methyl furan-2-carboxylate (0.98 g, 7.8 mmol) to THF solution in which acetyl-TPE (1 g, 2.6 mmol) is dissolved, then NaH (60% 0.16 g, 3.9 mmol) was quickly added, and the mixture was heated to 75 °C in an oil bath under argon and refluxed for 12 h. TLC detection reaction progress (petroleum ether/ethyl acetate = 15/1). After completion of the reaction, the reaction solution was cooled to room temperature, and added diluted hydrochloric acid, poured into ice water, extracted with dichloromethane, and organic layer was collected. The organic layer was dried over anhydrous Na_2SO_4, the solvent was removed under reduced pressure, brown oily β-diketone precursor was obtained. The β-diketone precursor was dried under vacuum and then dissolved in 5 ml of acetone, added K_2CO_3 (1.1eq), NaI (1.1eq), benzyl bromide (1.2eq) to the above solution, refluxed in argon atmosphere for 8 h. The crude product was purified by column chromatography (silica gel, 8:1 v/v, petroleum ether/ethyl acetate) to afford product **TPE-BF** as orange solid, yield 60%, m.p. 152.3–153.8 °C. ^{1}H NMR (400 MHz, $CDCl_3$) δ 7.66 (d, J = 8.5 Hz, 2H), 7.48 (d, J = 2.1 Hz, 1H), 7.25–6.95 (m, 23H), 6.48 (dd, J = 3.6, 1.7 Hz, 1H), 5.28 (t, J = 6.9 Hz, 1H), 3.44–3.30 (m, 2H) (Fig. S7). ^{13}C NMR (101 MHz, $CDCl_3$) δ 194.52, 184.16, 151.89, 149.42, 146.74, 143.13, 143.03, 142.93, 142.86, 139.68, 138.83, 133.94, 131.66, 131.31, 131.28, 131.23, 129.08, 128.48, 128.13, 127.90, 127.88, 127.73, 126.98, 126.84, 126.81, 126.53, 118.37, 112.71, 59.15, 34.94 (Fig. S8). HRMS (MALDI-TOF): m/z 581.2089, $[M+Na]^+$, calculated 581.2087 (Fig. S11).

4.2. 2-Benzyl-1-(thiophen-2-yl)-3-(4-(1,2,2-triphenylvinyl)phenyl) propane-1,3-dione (TPE-BT)

Compound **TPE-BT** was prepared by following the synthetic procedure for compound **TPE-BF**.

Methyl thiophene-2-carboxylate was condensed with acetyl-TPE to give β-diketone. The β-diketone precursor was dried under vacuum and then dissolved in 5 ml of acetone, added K_2CO_3, NaI and benzyl bromide to the above solution, refluxed in argon atmosphere for 8 h. The crude product was purified by column chromatography (silica gel, 8:1 v/v, petroleum ether/ethyl acetate) to afford product **TPE-BT** as orange solid, yield 63%, m.p. 153.8–155.8 °C. ^{1}H NMR (400 MHz, $CDCl_3$) δ 7.69–7.56 (m, 4H), 7.25–6.94 (m, 23H), 5.21 (t, J = 6.9 Hz, 1H), 3.42 (t, J = 6.7 Hz, 2H) (Fig. S9). ^{13}C NMR (101 MHz, CDCl3) δ 194.29, 188.01, 149.53, 143.42, 143.10, 142.99, 142.92, 142.88, 139.64, 138.86, 134.69, 133.82, 132.83, 131.73, 131.31, 131.26, 131.23, 129.05, 128.56, 128.32, 128.14, 127.90, 127.88, 127.72, 127.01, 126.84, 126.81, 126.63, 60.87, 35.66 (Fig. S10). HRMS (MALDI-TOF): m/z 597.1856, $[M+Na]^+$, calculated 597.1859 (Fig. S12).

Declaration of competing interest

The authors declare that they have no known competing financial interests or personal relationships that could have appeared to influence the work reported in this paper.

Data availability

No data was used for the research described in the article.

Acknowledgements

This work was supported by the Guangxi Natural Science Foundation (Grant No. 2020GXNSFAA159147) and National Natural Science Foundation of China (Grant Nos. 21766030 and 21566034).

Appendix A. Supplementary data

Supplementary data to this article can be found online at https://doi.org/10.1016/j.tet.2023.133355.

References

[1] (a) R. Bishop, Chem. Soc. Rev. 25 (1996) 311–319;
(b) F.C. Pigge, CrystEngComm 13 (2011) 1733–1748;
(c) V. Jayant, D. Das, Cryst. Growth Des. 16 (2016) 4183–4189.
[2] (a) D.E. Braun, T. Gelbrich, V. Kahlenberg, U.J. Griesser, CrystEngComm 17 (2015) 2504–2516;
(b) C.E.S. Bernardes, M.E. Minas da Piedade, Cryst. Growth Des. 12 (2012) 2932–2941;
(c) A. Llinas, J.M. Goodman, Drug Discov. Today 13 (2008) 198–210.

[3] (a) J. Yang, Z. Ren, B. Chen, M. Fang, Z. Zhao, B.Z. Tang, Q. Peng, Z. Li, J. Mater. Chem. C 5 (2017) 9242–9246;
(b) Y. Dong, J. Zhang, X. Tan, L. Wang, J. Chen, B. Li, L. Ye, B. Xu, B. Zou, W. Tian, J. Mater. Chem. C 1 (2013) 7554–7559;
(c) Q. Liao, Z. Wang, Q. Gao, Z. Zhang, J. Ren, J. De, X. Zhang, Z. Xu, H. Fu, J. Mater. Chem. C 6 (2018) 7994–8002.
[4] (a) Z. Wang, X. Cheng, A. Qin, H. Zhang, J.Z. Sun, B.Z. Tang, J. Phys. Chem. B 122 (2018) 2165–2176;
(b) Y. Zhou, J. Hua, B.Z. Tang, Y. Tang, Sci. China Chem. 62 (2019) 1312–1332;
(c) J. Yang, Z. Chi, W. Zhu, B.Z. Tang, Z. Li, Sci. China Chem. 62 (2019) 1090–1098;
(d) Z. Yang, Z. Chi, Z. Mao, Y. Zhang, S. Liu, J. Zhao, M.P. Aldred, Z. Chi, Mater. Chem. Front. 2 (2018) 861–890;
(e) Z. Wang, Y. Li, D. Yuan, L. Qian, L. Li, H. Wu, M. Liu, J. Ding, X. Huang, Dyes Pigments 162 (2019) 203–213.
[5] (a) C. Wang, Z. Li, Mater. Chem. Front. 1 (2017) 2174–2194;
(b) Q. Sun, K. Zhang, Z. Zhang, L. Tang, Z. Xie, Z. Chi, S. Xue, H. Zhang, W. Yang, Chem. Commun. 54 (2018) 8206–8209;
(c) Y. Hou, J. Du, J. Hou, P. Shi, T. Han, Y. Duan, J. Lumin. 204 (2018) 221–229;
(d) Q. Li, Z. Li, Accounts Chem. Res. 53 (2020) 962–973;
(e) Y. Hou, J. Du, J. Hou, P. Shi, K. Wang, S. Zhang, T. Han, Z. Li, Dyes Pigments 160 (2019) 830–838;
(f) P. Shi, Y. Duan, W. Wei, Z. Xu, Z. Li, T. Han, J. Mater. Chem. C 6 (2018) 2476–2482.
[6] (a) Z. Xie, T. Su, E. Ubba, H. Deng, Z. Mao, T. Yu, T. Zheng, Y. Zhang, S. Liu, Z. Chi, J. Mater. Chem. C 7 (2019) 3300–3305;
(b) Y. Qi, N. Ding, Z. Wang, L. Xu, Y. Fang, ACS Appl. Mater. Interfaces 11 (2019) 8676–8684;
(c) R. Zhao, L. Zhao, M. Zhang, Z. Li, Y. Liu, T. Han, Y. Duan, K. Gao, Dyes Pigments 167 (2019) 181–188.
[7] (a) S. Zeng, H. Sun, C. Park, M. Zhang, M. Zhu, M. Yan, N. Chov, E. Li, A.T. Smith, G. Xu, S. Li, Z. Hou, Y. Li, B. Wang, D. Zhang, L. Sun, Mater. Horiz. 7 (2020) 164–172;
(b) B. Li, H. Ge, Sci. Adv. 5 (2019);
(c) X. Yang, Q. Wang, P. Hu, C. Xu, W. Guo, Z. Wang, Z. Mao, Z. Yang, C. Liu, G. Shi, L. Chen, B. Xu, Z. Chi, Mater. Chem. Front. 4 (2020) 941–949;
(d) Y. Zhang, H. Xu, W. Xu, C. Zhang, J. Shi, B. Tong, Z. Cai, Y. Dong, Sci. China Chem. 62 (2019) 1393–1397;
(e) J.D. Luo, Z.L. Xie, J.W.Y. Lam, L. Cheng, H.Y. Chen, C.F. Qiu, H.S. Kwok, X.W. Zhan, Y.Q. Liu, D.B. Zhu, B.Z. Tang, Chem. Commun. (2001) 1740–1741.
[8] (a) W. Liu, Y. Wang, G. Ge, L. Ma, Dyes Pigments (2019) 171;
(b) Y. Wang, W. Liu, L. Ren, G. Ge, Mater. Chem. Front. 3 (2019) 1661–1670;
(c) W. Liu, Y. Wang, J. Yang, X. Li, X. Wang, L. Ma, Dyes Pigments (2020) 175.
[9] (a) A. Costa, E.R. Costa, A.L. Pereira Silva, A.A. Tanaka, J.d.J. Gomes Varela Junior, J. Mol. Model. (2018) 24;
(b) M.-H. Yang, D.L. Orsi, R.A. Altman, Angew. Chem.-Int. Edit. 54 (2015) 2361–2365.
[10] C. Deng, S. Zheng, D. Wang, J. Yang, Y. Yue, M. Li, Y. Zhou, S. Niu, L. Tao, T. Tsuboi, J. Phys. Chem. C 123 (2019) 29875–29883.
[11] T. Butler, F. Wang, M. Sabat, C.L. Fraser, Mater. Chem. Front. 1 (2017) 1804–1817.
[12] L.S. Rohwer, J.E. Martin, J. Lumin. 115 (2005) 77–90.
[13] (a) P.Z. Chen, L.Y. Niu, Y.Z. Chen, Q.Z. Yang, Coord. Chem. Rev. 350 (2017) 196–216;
(b) J. Samonina-Kosicka, C.A. DeRosa, W.A. Morris, Z. Fan, C.L. Fraser, Macromolecules 47 (2014) 3736–3746.
[14] Y.P. Qi, W.J. Liu, Y.T. Wang, L. Ma, Y.J. Yu, Y. Zhang, L.T. Ren, New J. Chem. 42 (2018) 11373–11380.